IL NUOVO CIMENTO **38 C** (2015) 148
DOI 10.1393/ncc/i2015-15148-4

COLLOQUIA: LaThuile15

Higgs boson couplings to bosons with the ATLAS detector: Run 1 legacy

E. PETIT on behalf of the ATLAS COLLABORATION
DESY - Hamburg and Zeuthen, Germany

received 2 October 2015

Summary. — The final ATLAS measurements of Higgs boson production and couplings in the decay channels $H \to ZZ^{(*)} \to \ell\ell\ell\ell$, $H \to \gamma\gamma$ and $H \to WW^{(*)} \to \ell\nu\ell\nu$ are presented, based on the run 1 of the LHC. The analyses are optimised to measure the number of observed Higgs boson decays divided by the corresponding Standard Model predictions for individual Higgs boson production processes. Total, fiducial and differential cross-sections are also measured. No significant deviations from the predictions of the Standard Model are found.

PACS 14.80.Bn – Standard-model Higgs bosons.

1. – Introduction

In July 2012, the ATLAS [1] and CMS [2] collaborations independently reported the observation of a new particle [3, 4] compatible with the Standard Model Higgs boson. Among the measurements of the properties of this new boson, the strengths of its couplings to fermions and vectors bosons are of primary interest. These couplings, depending on the value of m_H, can be tested by measurements of ratios of the number of observed events produced through the main production modes in the different decay channels to the corresponding Standard Model predictions. Those ratios are called *signal strengths* μ.

At the LHC the Higgs bosons are mainly produced through gluon fusion (ggF), weak vector-boson fusion (VBF) and associated production with a W boson (WH), a Z boson (ZH) or a top-quark pair ($t\bar{t}H$). Those processes are depicted in fig. 1. The ggF and $t\bar{t}H$ processes are sensitive to the couplings of the Higgs boson to fermions while the VBF and VH ($WH + ZH$) ones are sensitive to the couplings to vector bosons.

This note presents the final measurements with data collected during the run 1 of the LHC of the Higgs boson decaying to bosons [5-7], based on the proton-proton collision datasets corresponding to integrated luminosities of $4.5\,\text{fb}^{-1}$ collected by the ATLAS detector at $\sqrt{s} = 7\,\text{TeV}$ and $20.3\,\text{fb}^{-1}$ collected at $\sqrt{s} = 8\,\text{TeV}$ at the LHC. The decays

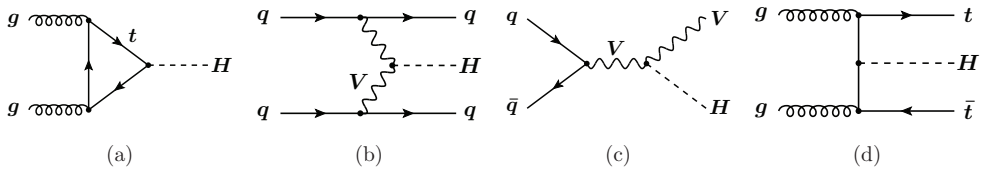

(a) (b) (c) (d)

Fig. 1. – Feynman diagrams for the leading production modes: (a) ggF, (b) VBF, (c) $VH = WH + ZH$ and (d) $t\bar{t}H$.

to fermions are discussed in [8]. All the results presented here are obtained for a Higgs boson mass $m_H = 125.36\,\text{GeV}$ measured by ATLAS using the combination of results from the decay channels $H \to \gamma\gamma$ and $H \to ZZ^{(*)} \to \ell\ell\ell\ell$ [9].

2. – Selection and background estimate

2˙1. *$H \to ZZ^{(*)} \to \ell\ell\ell\ell$ channel.* – The analysis [5] is based on the selection of two same flavour, opposite sign lepton pairs. The four leptons are required to be well identified and isolated with a transverse momentum $p_{\text{T}} > 20$, 15, 10 and 7 (electron)/6 (muon) GeV, respectively. The lepton pair with invariant mass closest to the Z boson mass must have an invariant mass m_{12} between 50 and 106 GeV. The requirement on the other lepton pair is relaxed because the second Z boson must be off-shell for a 125 GeV Higgs boson; its invariant mass m_{34} has to be between 12 and 115 GeV. The resolution is improved by including final-state radiation photons in the four-lepton event, and by recomputing the lepton four-momenta of the leading dilepton pair by means of a Z-mass constrained kinematic fit.

The irreducible background $ZZ^{(*)}$ is estimated from the Monte Carlo prediction and normalised to the theoretical cross-section. The reducible background, mainly $Z + jets$ and $t\bar{t}$, is estimated from data-driven measurements, depending of the flavour of the sub-leading lepton pair. After selection, in the $120 < m_{4l} < 130\,\text{GeV}$ mass region, 16.2 signal events are expected, as well as 7.4 and 3.0 irreducible and reducible background events respectively. In total 37 data events are observed.

2˙2. *$H \to \gamma\gamma$ channel.* – In the $H \to \gamma\gamma$ channel [6], a few hundred signal events are expected, but this channel has to deal with a large irreducible (γ-γ) and reducible (γ-*jet* and *dijet*) background, with a signal over background ratio of a few percent. Two well identified and isolated photons with $E_{\text{T}} > 0.35 * m_{\gamma\gamma}$ and $0.25 * m_{\gamma\gamma}$ for the leading and subleading photons are required. The fraction of genuine diphoton events is around 75%.

In order to increase the sensitivity, the dataset is divided into 12 exclusive event categories with different signal over background ratios and different diphoton invariant mass resolutions.

The signal is then extracted with an extended likelihood fit built from the number of observed events and analytical functions describing the distributions of $m_{\gamma\gamma}$ in the range 105–160 GeV for the signal and the background. After selection 422 signal events are expected and 13196 background events are observed in a window containing 90% of the signal.

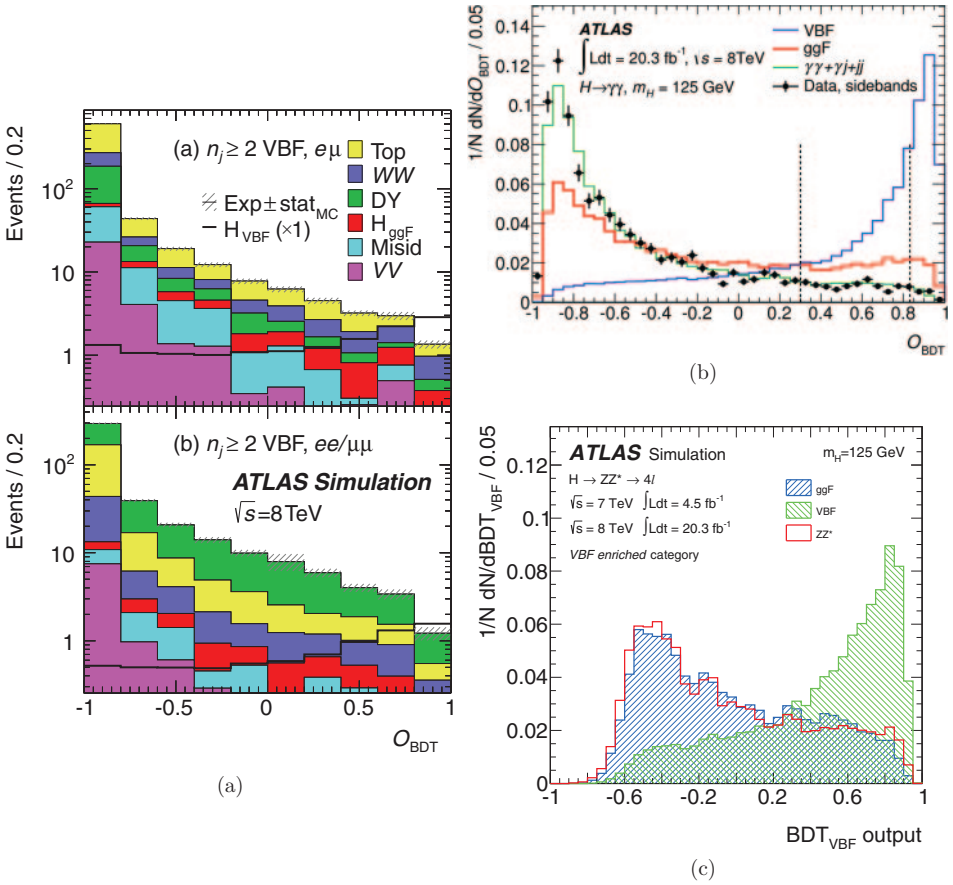

Fig. 2. – BDT discriminant outputs O_{BDT} of the VBF signal and the different backgrounds in the (a) $H \to WW^{(*)} \to \ell\nu\ell\nu$ [7], (b) $H \to \gamma\gamma$ [6] and (c) $H \to ZZ^{(*)} \to \ell\ell\ell\ell$ [5] channels, respectively.

2˙3. *$H \to WW^{(*)} \to \ell\nu\ell\nu$ channel.* – In the $H \to WW^{(*)} \to \ell\nu\ell\nu$ channel [7], a few hundred signal events are expected, with a signal-over-background ratio up to 10%; but because of neutrinos in the final state, it is not possible to reconstruct completely the event. The transverse mass constructed from the leptons and the missing transverse momentum is used as the discriminating variable. Two good isolated leptons with a transverse momentum larger than 22 and 10 GeV respectively are selected. Several cuts are made to reject the Drell-Yan and $t\bar{t}$ backgrounds, such as cuts on the missing transverse momentum or the transverse mass of the leptons. Cuts are also made to separate between WW and Higgs boson events, making use of the spin correlations: the leptons tend to be emitted in the same direction for the latter case.

The events are then divided into exclusive event categories depending the flavour of the lepton and the number of jets.

The number of background events in each category is extracted using shapes from Monte Carlo samples and normalised to the number of events in data in control regions enriched in the targeted background.

TABLE I. – *Number of expected and observed events in the categories enriched in VBF, as well as fraction of VBF events. The numbers of background events in the $H \to ZZ^{(*)} \to \ell\ell\ell\ell$ [5] and $H \to WW^{(*)} \to \ell\nu\ell\nu$ [7] channels correspond to expected events while the numbers in the $H \to \gamma\gamma$ channel are measured by fits to the data. The different categories correspond to different cuts on the output value of the BDT.*

$\sqrt{s}$	Channel	Category	N_{sig}	$N_{\text{VBF}}/N_{\text{Higgs}}$	N_{bkg}	N_{obs}
$7+8\,\text{TeV}$	$H \to ZZ^{(*)} \to \ell\ell\ell\ell$	cat 1	1.13	55%	0.16	1
$7+8\,\text{TeV}$	$H \to \gamma\gamma$	cat 1	11.0	60%	44.0	-
		cat 2	6.7	80%	6.7	-
$8\,\text{TeV}$	$H \to WW^{(*)} \to \ell\nu\ell\nu$	cat 1	12.5	60%	82.0	90
		cat 2	10.0	80%	14.9	28
		cat 3	6.5	90%	2.3	12

3. – Categorisation

In order to separate the different production modes the selected events are divided into exclusive categories enriched in the production modes:

- $H \to ZZ^{(*)} \to \ell\ell\ell\ell$ channel: one category enriched in the VBF process, two categories enriched in the VH process, one untagged category;
- $H \to \gamma\gamma$ channel: two categories enriched in the $t\bar{t}H$ process([1]), four categories enriched in the VH process, two categories enriched in the VBF process and four untagged categories;
- $H \to WW^{(*)} \to \ell\nu\ell\nu$ channel: one 2-jet category enriched in the VBF process, one 2-jet category enriched in the ggF process, two 0-jet and 1-jet categories.

3˙1. *Vector Boson Fusion process.* – Signal events produced by the VBF mechanism are characterised by two well-separated jets with high transverse momentum and little hadronic activity between them. In the three channels a multivariate analysis exploits the full event topology by combining different variables into a single discriminant that takes into account the correlations among them. The final BDT discriminant outputs for the three channels can be seen in fig. 2. One VBF category is defined in the $H \to ZZ^{(*)} \to \ell\ell\ell\ell$ channel by cutting on the output value of the BDT, two in the $H \to \gamma\gamma$ channel and three in the $H \to WW^{(*)} \to \ell\nu\ell\nu$ channel.

The number of expected and observed signal and background events, as well as the fraction of VBF events in the total expected signal events are summarised in table I for the VBF categories. This fraction is always larger than 50%.

3˙2. *Associated VH production.* – The categories enriched in the associated VH production process are defined by the decay of the associated vector boson. In the $H \to ZZ^{(*)} \to \ell\ell\ell\ell$ channel two categories are defined, enriched in two-jet events or containing one additional lepton. In the $H \to \gamma\gamma$ channels four categories are defined,

([1]) Discussed in ref. [8]

TABLE II. – *Number of expected and observed events in the categories enriched in VH, as well as fraction of VH events. The numbers of background events in the $H \to ZZ^{(*)} \to \ell\ell\ell\ell$ [5] and $H \to WW^{(*)} \to \ell\nu\ell\nu$ [7] correspond to expected events while the numbers in the $H \to \gamma\gamma$ [6] channel are measured by fits to the data.*

$\sqrt{s}$	Channel		N_{sig}	N_{VH}/N_{Higgs}	N_{bkg}	N_{obs}
$7+8\,\text{TeV}$	$H \to ZZ^{(*)} \to \ell\ell\ell\ell$	2 jets	0.64	33%	0.18	0
		1 lepton	0.08	84%	0.03	0
$7+8\,\text{TeV}$	$H \to \gamma\gamma$	2 leptons	0.4	99%	0.27	-
		1 lepton+$E_{\text{T}}^{\text{miss}}$	2.0	96%	4.4	-
		0 lepton +$E_{\text{T}}^{\text{miss}}$	1.4	88%	3.2	-
		2 jets	3.8	49%	18	-

containing two leptons, one lepton and missing transverse momentum ($E_{\text{T}}^{\text{miss}}$), zero leptons and missing transverse momentum, or two jets.

The number of expected and observed signal and background events, as well as the fraction of VH events in the total expected signal events are summarised in table II. This fraction is higher than 85% in categories with leptons.

4. – Results

4˙1. *Global results*. – In the $H \to ZZ^{(*)} \to \ell\ell\ell\ell$ channel the mass and signal strength are extracted from a 2D fit to the four-lepton invariant mass and a BDT output designed to distinguish signal from ZZ^* background. The observed (expected) local significance at $m_H = 125.36\,\text{GeV}$ is 8.1σ (6.2σ), corresponding to a signal strength $\mu = 1.50^{+0.35}_{-0.31}(\text{stat})^{+0.19}_{-0.13}(\text{syst})$.

In the $H \to \gamma\gamma$ channel the observed (expected) local significance at $m_H = 125.36\,\text{GeV}$ is 5.2σ (4.6σ), corresponding to a signal strength $\mu = 1.17^{+0.23}_{-0.23}(\text{stat})^{+0.10}_{-0.08}(\text{syst})^{+0.12}_{-0.08}(\text{theo})$.

In the $H \to WW^{(*)} \to \ell\nu\ell\nu$ channel a binned likelihood fit is simultaneously performed on all categories in order to extract the signal from the backgrounds and measure its yield. The observed (expected) local significance at $m_H = 125.36\,\text{GeV}$ is 6.1σ (5.8σ), corresponding to a signal strength $\mu = 1.09^{+0.16}_{-0.15}(\text{stat})^{+0.17}_{-0.14}(\text{syst})$.

4˙2. *Coupling results*. – The signal strengths per production mode are summarised in table III. All values are compatible with Standard Model expectations.

TABLE III. – *Signal strength per production mode for the three bosonic decay channels* [5-7].

	$H \to ZZ^{(*)} \to \ell\ell\ell\ell$	$H \to \gamma\gamma$	$H \to WW^{(*)} \to \ell\nu\ell\nu$
ggF	$1.7^{+0.5}_{-0.4}$	1.32 ± 0.38	$1.02^{+0.29}_{-0.26}$
VBF	$0.3^{+1.6}_{-0.9}$	0.8 ± 0.7	$1.27^{+0.53}_{-0.45}$
WH		1.0 ± 1.6	
ZH		$0.1^{+3.7}_{-0.1}$	
$t\bar{t}H$		$1.6^{+2.7}_{-1.8}$	

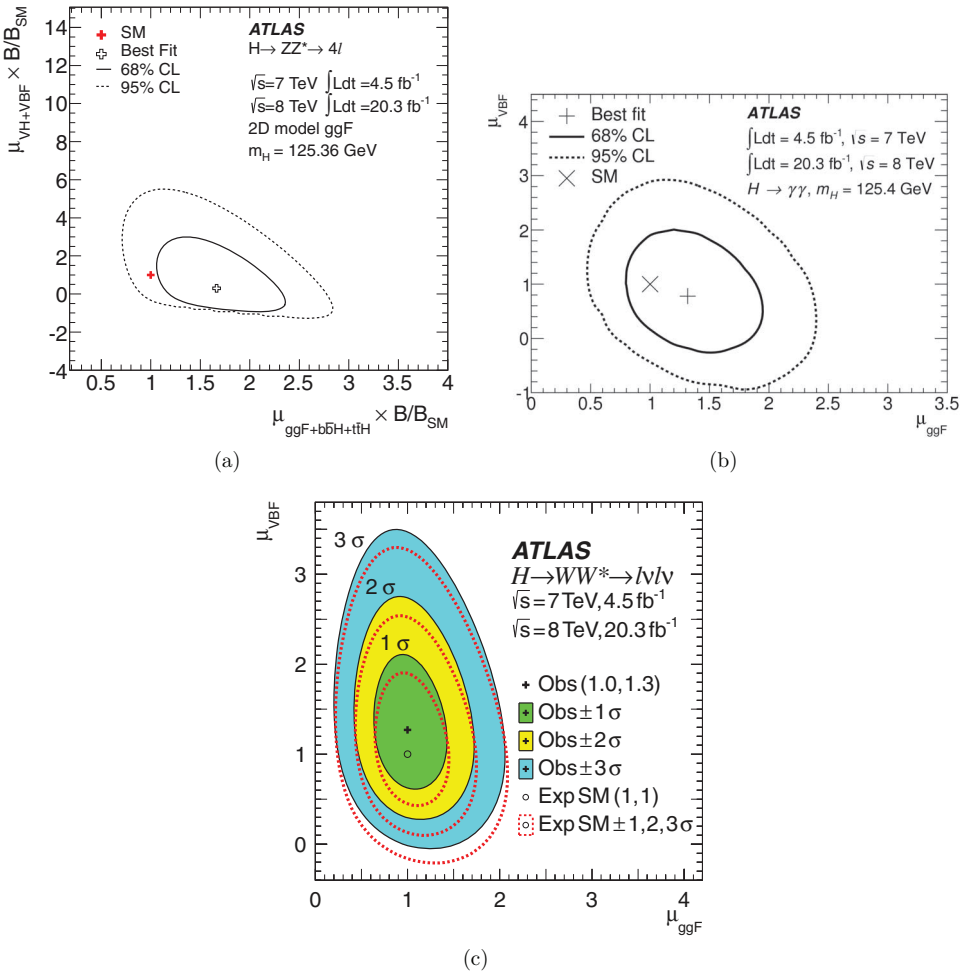

Fig. 3. – The two-dimensional best-fit value of ($\mu_{\rm VBF}$,$\mu_{\rm ggF}$) for the (a) $H \to ZZ^{(*)} \to \ell\ell\ell\ell$ [5], (b) $H \to \gamma\gamma$ [6] and (c) $H \to WW^{(*)} \to \ell\nu\ell\nu$ [7] channels, respectively.

The correlation between the fitted values of $\mu_{\rm ggF}$ and $\mu_{\rm VBF}$ are shown in fig. 3 where the best-fit values and the 68% and 95% CL contours are shown for the three decay channels.

In order to test the production through VBF independently of the branching ratios, the ratio $\mu_{\rm VBF}/\mu_{\rm ggF}$ is fitted separately by profiling the remaining signal strengths. The value of the likelihood at $\mu_{\rm VBF}/\mu_{\rm ggF} = 0$ can be interpreted as the observed significance of the VBF process. For the $H \to WW^{(*)} \to \ell\nu\ell\nu$ channel it corresponds to 3.2 standard deviation (2.7 expected), establishing the evidence for the VBF production mode.

4˙3. *Cross-section measurements.* – The measurement of fiducial and differential cross-sections [10,11] is an alternative approach to studying the properties of the Higgs boson and allows a diverse range of physical phenomena to be probed, such as the theoretical modelling of different Higgs boson production mechanisms and physics beyond the Stan-

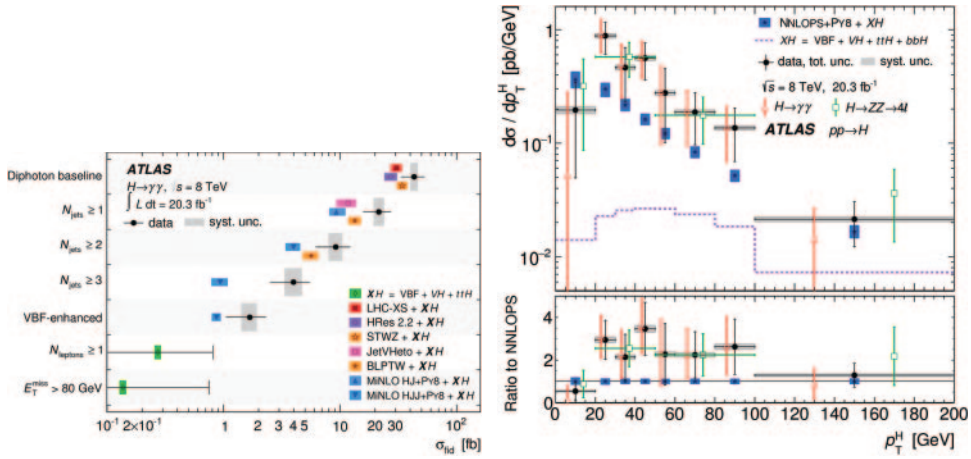

(a) (b)

Fig. 4. – (a) Measured cross-sections and cross-section limits in seven fiducial regions in the $H \to \gamma\gamma$ channel. The data are compared to state-of-the-art theoretical predictions [11]. (b) Differential cross-section of the Higgs boson transverse momentum measured in the $H \to \gamma\gamma$ and $H \to ZZ^{(*)} \to \ell\ell\ell\ell$ final states [12]. Both the combined measurements as well as the individual channels are shown, compared to predictions from the Monte Carlo event generators NNLOPS [13, 14]+PYTHIA8 [15] for the ggF process, POWHEG [16-18] interfaced with PYTHIA8 for the VBF process and PYTHIA8 for the other processes.

dard Model. Furthermore, the cross-sections are designed to be as model independent as possible to allow comparison to any current or future theoretical prediction. Fiducial cross-sections are computed in the three bosonic decay channels. Figure 4(a) shows an example of cross-sections measured in the $H \to \gamma\gamma$ channel in different fiducial regions. All measurements are compatible with the Standard Model expectations; for events containing at least three jets in addition to the diphoton system, the prediction is below the data by 2.1σ significance.

Differential cross-sections measured in the $H \to ZZ^{(*)} \to \ell\ell\ell\ell$ and $H \to \gamma\gamma$ channels are statistically limited and have comparable total uncertainties. Combining the analyses improves the precision of the cross-section measurements by up to 40% (typically 25–30%). An example of individual and combined measurements of the Higgs boson transverse momentum is shown in fig. 4(b).

5. – Conclusion

The final ATLAS results on the study of the Higgs boson decaying into bosons with run 1 data were shown. The data is divided into categories enriched in production modes which allows the computation of signal strengths per production mode. These results are then used as an input to a global combination to test the Higgs boson couplings. Total, fiducial and differential cross-sections are also measured. All measurements are compatible with the Standard Model expectations.

REFERENCES

[1] ATLAS Collaboration, *JINST*, **3** (2008) S08003.
[2] CMS Collaboration, *JINST*, **3** (2008) S08004.
[3] ATLAS Collaboration, *Phys. Lett. B*, **716** (2012) 1.
[4] CMS Collaboration, *Phys. Lett. B*, **716** (2012) 30.
[5] ATLAS Collaboration, *Phys. Rev. D*, **91** (2015) 012006.
[6] ATLAS Collaboration, *Phys. Rev. D*, **90** (2014) 112015.
[7] ATLAS Collaboration, *Phys. Rev. D*, **92** (2015) 012066.
[8] Filthaut F. on behalf of the ATLAS Collaboration, *Measurement of Higgs couplings to fermions in the ATLAS experiment*, talk presented at this Conference.
[9] ATLAS Collaboration, *Phys. Rev. D*, **90** (2014) 052004.
[10] ATLAS Collaboration, *Phys. Lett. B*, **738** (2014) 234–253.
[11] ATLAS Collaboration, *JHEP*, **1409** (2014) 112.
[12] ATLAS Collaboration, *Phys. Rev. Lett.*, **115** (2015) 091801.
[13] Hamilton K., Nason P., Re E. and Zanderighi G., *JHEP*, **1310** (2013) 222.
[14] Catani S. and Grazzini M., *Phys. Rev. Lett.*, **98** (2007) 222002.
[15] Sjostrand T., Mrenna S. and Skands P. Z., *Comput. Phys. Commun.*, **178** (2008) 852.
[16] Nason P., *JHEP*, **0411** (2004) 040.
[17] Frixione S., Nason P. and Oleari C., *JHEP*, **0711** (2007) 070.
[18] Aliolo S., Nason P., Oleari C. and Re E., *JHEP*, **1006** (2010) 043.